Site-selective doublon-holon dynamics in a pumped one-dimensional Hubbard superlattice with staggered Coulomb interactions

Zhenyu Cheng,[1] Ying Li,[1] Hantao Lu,[2] Xiang Hu,[1] Zhongbing Huang,[3] Gregory A. Fiete,[4,5] and Liang Du[1,*]

[1]*College of Physics and Technology, Guangxi Normal University, Guilin, Guangxi 541004, China*

[2]*Lanzhou Center for Theoretical Physics, Key Laboratory of Theoretical Physics of Gansu Province, and Key Laboratory of Quantum Theory and Applications of MoE, Lanzhou University, Lanzhou, Gansu 730000, China*

[3]*Department of Physics, Hubei University, Wuhan 430062, China*

[4]*Department of Physics, Northeastern University, Boston, Massachusetts 02115, USA*

[5]*Department of Physics, Massachusetts Institute of Technology, Cambridge, Massachusetts 02139, USA*

(Received 25 November 2023; revised 4 February 2024; accepted 25 April 2024; published 7 May 2024)

Doublon-holon dynamics is investigated in a pumped one-dimensional Hubbard model with a staggered on-site Coulomb interaction at half-filling. When the system parameters are set to be in the Mott-insulating regime the equilibrium sublattice density of states exhibits several characteristic peaks, corresponding to the lower and upper Hubbard bands as well as hybridization bands. We study the linear absorption spectrum and find two main peaks characterizing the photon frequencies which excite the ground state to an excited state. For a system driven by a laser pulse with general intensity and frequency, both the energy absorption and the doublon-holon dynamics exhibit distinct behaviors as a function of laser amplitude and frequency. Single-photon processes are observed at low laser intensity where the energy is absorbed for resonant laser frequencies. For strong laser intensity multiphoton-induced dynamics are observed in the system that are confirmed by an evaluation of the Loschmidt amplitude. The contribution of multiphoton processes to site-resolved double occupancy is also characterized by the generalized Loschmidt amplitude. The site-resolved doublon-holon dynamics are observed in both the one and multiphoton processes and the site-resolved behavior is explained within a quasiparticle picture. Our study suggests strategies to optically engineer the doublon-holon dynamics in one-dimensional strongly correlated many-body systems.

DOI: 10.1103/PhysRevB.109.195121

I. INTRODUCTION

Nonequilibrium control of quantum states in strongly correlated systems with optical techniques and its physical understanding have been attracting attention from the condensed-matter community in the past decade and remains challenging [1–4]. Of particular interests are (1) thermalization and prethermalization behavior as the system is driven far from equilibrium [1,5], (2) nonthermal states not accessible in equilibrium [3,6,7], (3) nonequilibrium control of quantum phase transitions [2,4,8–11], and (4) disentangling degrees of freedom in a strongly correlated electronic system [12].

The doublon(doubly occupied states)-holon(emputy states) dynamics in the driven Hubbard model and its extended version in low (one- or two-) dimensional systems have attracted attention. In the one-dimensional extended Hubbard model, the doublon-holon pair is long lived and the expected decay mechanism due to spin excitation is inefficient [13,14]. A study of the doublon-holon dynamics on the photo-doped Mott insulator in the above system shows that the nonequilibrium system can be described as a generalized Gibbs ensemble [15]. In the pumped one-dimensional Hubbard model, the evolution of doubly occupied states (doublons) are dependent on the laser frequency [16–18]. Starting from a charge-density wave band insulator or a spin-density wave Mott insulator, doublon-holon pairs (exciton) will generate in-gap states in the optical conductivity [19,20]. On the other hand, in a two-dimensional Hubbard cluster, the system exhibits Rabi-like oscillations [21], where the oscillation frequency increases with the drive amplitude (intensity). In contrast to the one-dimensional case, the doublon dynamics in the Hubbard two-leg ladder exhibits weak coupling with magnetic excitations [22]. In addition, impact ionization is observed in a two-dimensional cluster [23–26] where the double occupancy rises further after the laser pulse.

The nonequilibrium studies summarized above are focused on systems with spatial homogeneity in the Hamiltonian. In such systems, doublons and holons are generated when a pump light is applied, which leads to an increase in the total energy of the system. After the passing of the pump light through the system, the system begins to relax through the recombination of doublons and holons, where prethermalization behavior occurs [15]. By contrast, the nonequilibrium dynamics in systems without spatial homogeneity (e.g., ionic Hubbard model, Hubbard superlattice with a staggered Coulomb interaction) have received relatively little attention. For the purpose of simplifying the physical picture and the analysis in nonequilibrium studies of doulon-holon dynamics, we focus our attention on the Hubbard superlattice with a

*Liang Du: liangdu@gxnu.edu.cn

FIG. 1. An example of a lattice with 10 sites, where the onsite Coulomb interaction strength is modulated alternatively (staggered) with $U_a \neq U_b$ for different sublattices.

staggered Coulomb potential rather than the ionic Hubbard model where charge-density wave, spin-density wave, and spontaneous dimerized states [27] could occur and complicate the analysis.

In this paper we focus on the nonequilibrium dynamics of the Hubbard superlattice with spatially staggered Coulomb interactions, as shown in Fig. 1. In equilibrium such a Hubbard superlattice can be experimentally realized in condensed-matter systems with nanoscale spatial inhomogeneity [28–33], which is characterized as a quasi-one-dimensional system with alternating atoms with varying on-site electron correlations and orbital energies. For example, the one-dimensional copper-oxide model [34] and the atomic chains of carbon-transitional-metal compounds [35] contain this essential physics. The simplest spatially inhomogeneous case is where there are two sites in the unit cell with on-site Coulomb interactions U_a for the A sublattice and U_b for the B sublattice. For a noninteracting B sublattice, $U_b = 0$, and finite $U_a > 0$ in one dimension, the system exhibits a correlated-metallic phase with zero spin and zero charge gaps [32,33] as the particle-hole symmetry is preserved. For a B sublattice with finite Coulomb interaction strength $U_b > 0$, the system is an antiferromagnetic Mott insulator with zero spin gap and finite charge gap [32]. Besides realizations in condensed-matter systems, a spatial modulation of the interaction has also been reported in ^{174}Yb gas systems [36], where the Coulomb interaction strengths can be tuned via a Feshbach resonance. The system undergoes a Mott metal-insulator transition as the Coulomb interaction increases [37–39] in the infinite-dimensional Bethe lattice, as shown within the framework of dynamical mean-field theory [40].

In this work, by introducing a spatial inhomogenity with spatially alternating (staggered) on-site Coulomb interactions, we study the doublon-holon dynamics as a function of laser intensity and frequency in the one-dimensional Hubbard superlattice with $U_b = 18.0t_h$, $U_b = 3.0t_h$ [see Eq. (1)], where the system is a Mott insulator before the pump is applied. We concentrate our investigation on the light-induced exotic electronic behavior, particularly as the system is driven into the far-from-equilibrium regime, where nonlinear phenomena, such as multiphoton processes, manifest. For weak laser intensity where linear response theory applies, we observe a site-selective doublon-holon dynamics at laser frequency $\hbar\Omega \approx 3.2t_h$, where the double occupancy of the B sublattice is enhanced by the laser pulse, while the double occupancy of the A sublattice remains almost unchanged during and after the laser pulse. With strong laser intensity, multiphoton effects are observed, and the site-selected doublon is observed for laser frequency at $\hbar\Omega = 9.4t_h$, with site A enhanced substantially while site B remains unchanged, in contrast to the selective behavior observed at $\hbar\Omega = 3.2t_h$. This observation opens the possibility to optically engineer doublon-holon states through appropriate laser protocol in many-body interacting systems.

Our paper is organized as follows. In Sec. II, we describe the Hamiltonian of the pumped one-dimensional Hubbard model with a modulated (staggered) site-dependent Coulomb interaction and the time-dependent Lanczos method of solution. In Sec. III, the equilibrium sublattice-resolved density of states and the linear absorption spectrum are obtained using exact diagonalization. In Sec. IV, we study the nonequilibrium dynamics of doublon-holons as a function of laser frequency and amplitude, and we study the eigenstate spectrum using the Loschmidt amplitude. In Sec. V, a generalized Loschmidt amplitude is introduced to exhibit details of the site-resolved doublon-holon dynamics. Finally, in Sec. VI we present the main conclusions of the paper.

II. MODEL AND METHOD

In equilibrium the one-dimensional Hubbard superlattice (A-B sublattice) with particle-hole symmetry is written as [32,33,41],

$$H = -t_h \sum_{i\sigma} (c^\dagger_{i\sigma} c_{i+1\sigma} + \text{H.c.}) + \sum_i U_i \left(n_{i\uparrow} - \frac{1}{2}\right)\left(n_{i\downarrow} - \frac{1}{2}\right), \tag{1}$$

where $c^\dagger_{i\sigma}$ ($c_{i\sigma}$) creates (annihilates) a fermionic particle at site i with spin projection σ and $n_{i\sigma} = c^\dagger_{i\sigma} c_{i\sigma}$ for $\sigma = \uparrow, \downarrow$. Here t_h is the hopping amplitude connecting nearest neighbor sites and U_i is the site-dependent onsite Coulomb interaction between $\uparrow$ and $\downarrow$ spin electrons, which we choose to be $U_i = U_a(U_b)$ for odd (even) sites in the one-dimensional chain.

In this paper, we set $t_h = 1$ as the energy unit and correspondingly, the unit of time is then the inverse of energy, t_h^{-1}. The site-specific density of states are defined as

$$\rho_\alpha(\omega) = \sum_{i\in\alpha,\sigma} \sum_\phi |\langle\phi|c^\dagger_{i\sigma}|\psi_0\rangle|^2 \delta(\omega - E_\phi + E_0) + |\langle\phi|c_{i\sigma}|\psi_0\rangle|^2 \delta(\omega + E_\phi - E_0), \tag{2}$$

where $\{|\phi\rangle\}$ are the eigenstates of the equilibrium Hamiltonian in Eq. (1) with respect to energy eigenvalues E_ϕ, and $|\psi_0\rangle$ is the ground state with energy E_0. The definition of the linear absorption spectrum is [18,42–44]

$$\alpha(\omega) = -\frac{1}{\pi} \text{Im} \langle\psi_0|\hat{j} \frac{1}{\omega + i\eta - (H - E_0)} \hat{j}|\psi_0\rangle, \tag{3}$$

where the broadening factor η is set as $\eta = 1/L$, with L the chain size. The current density operator is defined as

$$\hat{j} = it_h \sum_{i\sigma} (c^\dagger_{i\sigma} c_{i+1,\sigma} - c^\dagger_{i+1\sigma} c_{i,\sigma}). \tag{4}$$

The equation for linear absorption, Eq. (3), is only accurate in the low-laser-intensity regime, where linear response theory is applicable.

We consider a system exposed to an external laser pulse with vector potential (directed along the chain direction),

$$A(t) = A_0 \exp\left[-(t - t_p)^2/2t_d^2\right] \cos[\Omega(t - t_p)], \tag{5}$$

where A_0 is the laser intensity, Ω is the laser frequency, and the laser pulse is peaked at t_p, with t_d characterizing the duration time (pulse width) of light. We set $t_p = 8.0$, $t_d = 2.0$ in the following numerical calculations. The time-dependent Hamiltonian is written using the Peierls substitution,

$$H(t) = -t_h \sum_{i\sigma} \{\exp[iA(t)] c^\dagger_{i\sigma} c_{i+1\sigma} + \text{H.c.}\} + \sum_i U_i \left(n_{i\uparrow} - \frac{1}{2}\right)\left(n_{i\downarrow} - \frac{1}{2}\right). \quad (6)$$

We choose the chain size to be $L = 10$ with periodic boundary conditions and a coarse-grained time $\delta t = 0.005 t_h^{-1}$. In the following, we restrict ourselves to the case of half-filling with periodic boundary conditions, where the total number of electrons N is equal to the number of sites in the chain L. Furthermore, we assume the total magnetization in the system vanishes, which means the number of up-spin electrons $N_\uparrow$ is equal to the down-spin electrons $N_\downarrow$.

The exact diagonalization method (a standard Lanczos procedure) is employed to numerically calculate the ground state of the Hamiltonian at time $t = 0^-$, where the laser pulse is not yet applied to the system. The ground state is used as an initial state for the time-dependent Schrödinger equation, $i\partial_t |\Psi(t)\rangle = H(t)|\Psi(t)\rangle$. The time evolution is implemented step by step based on the time-dependent Lanczos method [16,42,45–47],

$$|\Psi(t+\delta t)\rangle \approx e^{-iH(t)\delta t}|\Psi(t)\rangle \approx \sum_{l=1}^{M} e^{-i\epsilon_l \delta t}|\Phi_l\rangle\langle\Phi_l|\Psi(t)\rangle,$$

where ϵ_l (Φ_l) are the eigenvalues (eigenvectors) of the tridiagonal matrix generated by Lanczos iteration with $M \leqslant 100$. (In general, the desired M for achieving a given accuracy depends on the setups and chosen time step size [48].) We set the time step size to be $\delta t = 0.005 t_h^{-1}$ in our calculation of the time evolution. The physical observables are computed as

$$\langle O(t)\rangle = \langle\Psi(t)|O|\Psi(t)\rangle. \quad (7)$$

For the case of high laser intensity, multiphoton processes appear or even dominate the optical excitations in the system. To validate the multiphoton processes and provide more details on the double-holon dynamics, the Loschmidt amplitude is used to calculate the spectral density [21,24,49],

$$L(\omega, t) = \sum_n |\langle E_n|\Psi(t)\rangle|^2 \delta[\omega - (E_n - E_g)], \quad (8)$$

where $|E_n\rangle$ and E_n are the eigenstates and eigenenergies (E_g is the many-body ground-state energy) of the unperturbed Hamiltonian (after the pulse Hamiltonian has decayed away) and $|\Psi(t)\rangle$ is the time evolved state at time t. Note that the eigenstate spectrum remains unchanged as a function of time after the pump pulse has decayed, because for these times $H(t) = H(0)$, and as a result $|\langle E_n|\Psi(t)\rangle|$ is unchanged.

III. DENSITY OF STATES AND LINEAR ABSORPTION SPECTRUM

In this section, we focus our attention on the Hubbard superlattice in the Mott-insulating phase with finite charge gap and zero spin gap [32], where the system parameters are $U_a = 18.0$ and $U_b = 3.0$ (measured in units of t_h). In Fig. 2(a), we plot the sublattice-resolved density of states in Eq. (2) at zero temperature using the Lanczos method. Evidently, the particle-hole symmetries are observed for both A and B sublattices, with each site singly occupied (half-filling). The energy gap at the Fermi energy ($E_F = 0.0$) confirms that the system is an insulator. Note the density of states exhibits four peaks for each sublattice. For the A sublattice, we observe the lower and upper Hubbard band are located approximately at $\pm U_a/2 = \pm 9.0$ and there are two hybridization bands around $\pm U_b/2 = \pm 1.5$. In contrast, the upper and lower Hubbard band for the B sublattice are located approximately at $\pm U_b/2 = \pm 1.5$ with tiny hybridization bands at $\pm U_a/2 = \pm 9.0$.

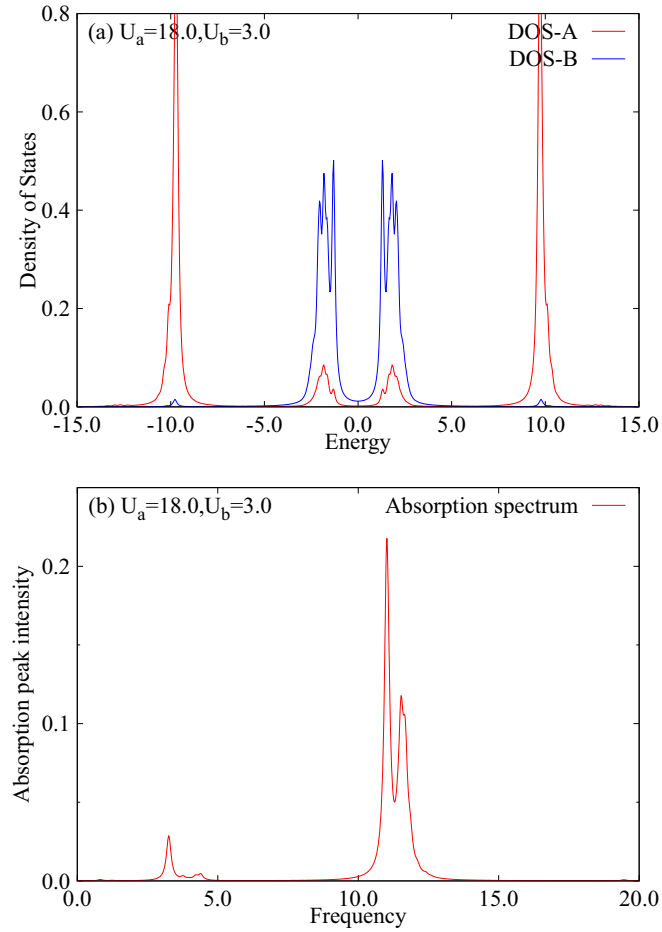

FIG. 2. Sublattice-resolved density of states for the Hubbard superlattice with fixed site-dependent Coulomb interaction strength $U_b = 3.0$ and $U_a = 18.0$. (a) The sublattice-resolved density of states in equilibrium. (b) The linear absorption spectrum as a function of frequency calculated using Eq. (3), where linear response theory applies. The broadening factor is set to $\eta = 0.1$ for both the density of states and the linear absorption spectrum.

To study the effect of a laser drive on the equilibrium system (taking it out of equilibrium), we first study the energy absorption of the superlattice system at low laser intensity where linear response theory applies. In Fig. 2(b), the linear absorption spectrum $\alpha(\omega)$ with $0.0 \leqslant \omega \leqslant 20.0$ is calculated

using Eq. (3), where Fermi's golden rule applies [26]. The positions of the peaks in the linear absorption spectrum (one-photon excited states) are $\omega \approx 3.2, 11.4$ (two peaks at $\omega \approx 11.0, 11.5$ are merged into a single peak). The peak at $\omega \approx 3.2$ corresponds to the energy difference between the lower Hubbard band of the B sublattice and the upper hybridization peak of the A sublattice or, inversely, from lower hybridization peak of A sublattice to the upper Hubbard band of B sublattice. The peak at $\omega \approx 11.4$ corresponds to the energy difference between the lower Hubbard band of the B sublattice and the upper Hubbard band of the A sublattice or, inversely, from lower Hubbard band of the A sublattice to the upper Hubbard band of the B sublattice. The physical picture can be clearly understood as follows: Since the hopping between the nearest-neighboring A-B sites is dominant, that process will contribute most to the optical excitation. In contrast, the next-nearest-neighbor A-A or B-B hopping, which is a second-order process (compared with the nearest-neighbor A-B first-order hopping process), is weaker.

IV. NONEQUILIBRIUM DRIVEN BEHAVIOR IN THE MOTT INSULATING REGIME

To gain an overall picture of photon absorption in the system, we plot the energy following the pulse ($t > 15.0$) as a function of laser frequency Ω and laser intensity A_0 in Fig. 3(a). Note the energy remains unchanged after the laser pulse has passed since the time evolution operator is unitary (no energy is being added or removed from the system). A linear response behavior is observed for small laser intensity for the one-photon resonance frequencies $\Omega \approx 3.2, 11.4$, which were clarified previously by the linear absorption spectrum in Fig. 2(b). To make the linear response regime clear, we plot the energy as a function of laser intensity with fixed laser frequency $\Omega = 3.2, 6.0, 9.4, 11.4$ in Fig. 3(b). The total energy exhibits linear energy absorption in the regime $A_0 < 0.20$ for laser frequencies $\Omega = 3.2, 11.4$. In contrast, the total energy does not change until $A_0 \geqslant 0.2$ for laser frequencies $\Omega = 6.0, 9.4$, which suggest single-photon absorption is absent for a lower-intensity laser and multiphoton excitation occurs for higher laser intensity.

To provide more details of the optical excitation process, we focus our attention on the nonequilibrium evolution of the total energy and double occupancy of the system. The time-dependent energy as a function of laser frequency is plotted in Figs. 4(a1), 4(b1), 4(c1), and 4(d1), where the laser intensities are set as $A_0 = 0.1, 0.2, 0.6, 1.0$, respectively. The time evolution of the site-resolved double occupancy is plotted in Figs. 4(a2) and 4(a3) for laser intensity $A_0 = 0.1$, Figs. 4(b2) and 4(b3) for $A_0 = 0.2$, Figs. 4(c2) and 4(c3) for $A_0 = 0.6$, and Figs. 4(d2) and 4(d3) for $A_0 = 1.0$.

For $A_0 = 0.1$ in the linear response regime, the photon energy is absorbed at frequency $\Omega = 11.4$ and a small energy absorption is observed at frequency $\Omega = 3.2$, which is consistent with the equilibrium calculation of the linear absorption spectrum in Fig. 2(b). By inspecting the site-resolved double occupancy as a function of time and laser frequency, we find that an increase of double occupancy on both the A site and the B site at frequency $\Omega = 11.4$ will contribute to the total energy absorption, while for laser frequency $\Omega = 3.2$, the energy absorption mainly comes from the enhancement of double occupancy only at the B site.

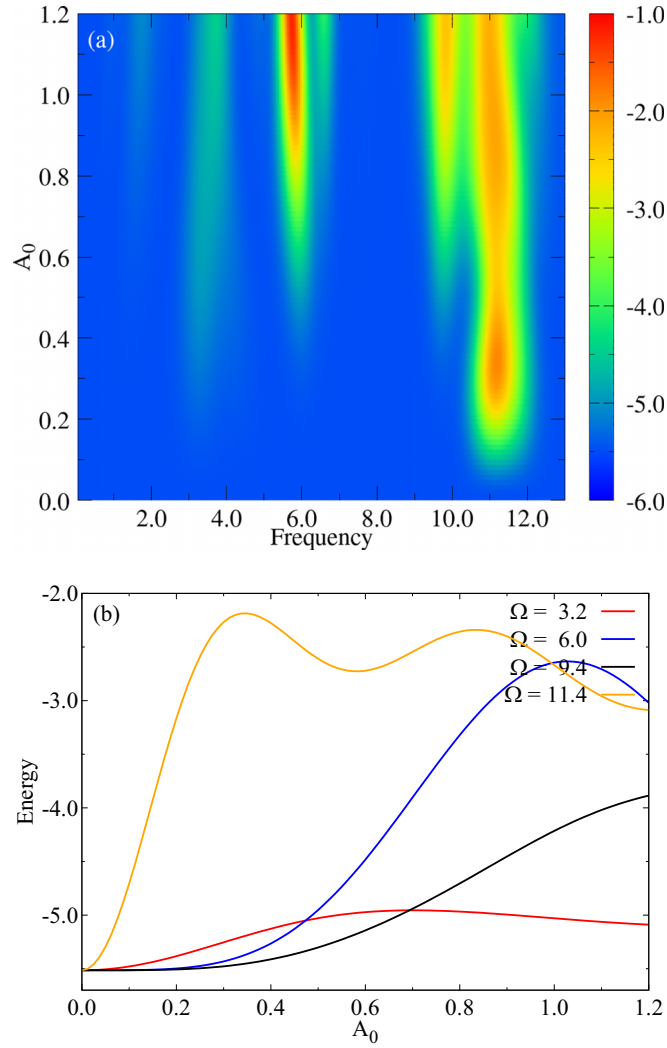

FIG. 3. The energy absorbed following the laser pulse for the Hubbard superlattice with fixed site-dependent Coulomb interaction strength $U_b = 3.0$ and $U_a = 18.0$. (a) The after-pulse ($t = 15.0$ used) energy as a function of laser frequency and amplitude. (b) The after-pulse energy as a function of laser amplitude with fixed laser frequency $\Omega = 3.2, 6.0, 9.4, 11.4$.

The behaviors above can be explained with the following physical picture: For laser frequency $\Omega = 11.4$, a single-photon absorption-induced optical excitation will move electrons from the lower Hubbard band of the A sublattice to the upper Hubbard band of the B sublattice, which enhances the double occupancy of the B site. Correspondingly, a photon can also excite electrons from the lower Hubbard band of the B sublattice to the upper Hubbard band of the A sublattice, enhancing the A-site double occupancy simultaneously.

By contrast, the physical picture is different for optical excitation with laser frequency $\Omega = 3.2$. A single-photon process will excite electrons from the lower Hubbard band of B sites to the upper hybridization band of A sites, enhancing the kinetic energy while not affecting the double occupancy of the A sites. However, an optical excitation from the lower

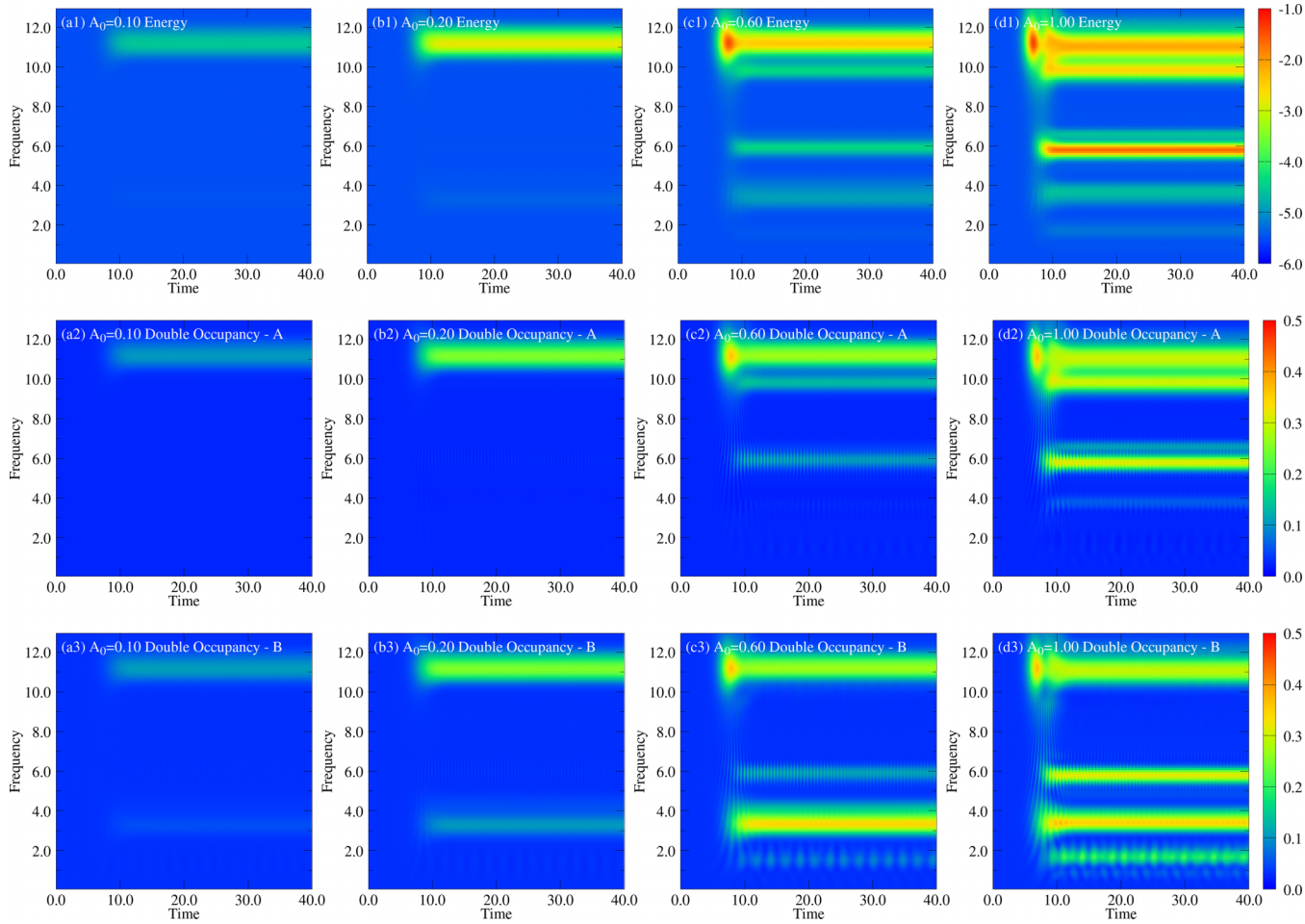

FIG. 4. The time evolution of the total energy and site-resolved double occupancy as a function of frequency Ω for the Hubbard superlattice with fixed site-dependent Coulomb interaction strength $U_b = 3.0$ and $U_a = 18.0$. The energy and site-resolved double occupancy is plotted with each column representing a different laser intensity $A_0 = 0.1$ [(a1)–(a3)], $A_0 = 0.2$ [(b1)–(b3)], $A_0 = 0.6$ [(c1)–(c3)], and $A_0 = 1.0$ [(d1)–(d3)].

hybridization A sites to the upper Hubbard bands of the B sublattice will enhance the double occupancy of the B sites. As a result, the system will exhibit site-selective doublon-holon dynamics at $\Omega = 3.2$ which results from a single-photon excitation. Further increasing the laser intensity to $A_0 = 0.2$ will not introduce new physics, except it enhances the effects observed with $A_0 = 0.1$, indicating that $A_0 = 0.2$ is still situated in the linear response region of optical excitation.

Increasing the laser intensity to $A_0 = 0.6$, besides the enhancement of energy absorption at $\Omega = 3.2, 11.4$ observed before, results in energy absorption at laser frequencies $\Omega = 9.4, 6.0, 1.5$ respectively. The extra absorption frequencies can be explained by multiphoton absorption processes, which indicate that $A_0 = 0.6$ is out of the linear response regime. For $\Omega = 6.0, 1.5$, the double-photon processes correspond to the excitation of single-photon process of $\Omega = 11.4, 3.2$, respectively (as the frequencies are roughly doubled). However, the two-photon process for $\Omega = 9.4$ is different from the other two frequencies, since we do not have an linear absorption peak at laser frequency $\Omega \approx 18.8$ in Fig. 2(b).

For $\Omega = 9.4$, an apparent enhancement of double occupancy is observed for the A site in Fig. 4(c2) while not for the B site in Fig. 4(c3). The short-time process is due to an excitation from the lower Hubbard band of the A sublattice to the upper Hubbard band of the B sublattice, which enhances the double occupancy of the B sites. At subsequent times, a quasiparticle is further excited to the upper Hubbard of the A sublattice, which results in a reduction of the double occupancy of the B sites and an increase of the A sites [see also Figs. 5(c1) and 5(c2)]. Thus, the double occupancy of the A sites is enhanced while the B sites do not change in the long-time regime (which is induced by the two-photon process in the relative long-time regime). Further increasing the laser intensity to $A_0 = 1.0$ will enhance the observed doublon-holon dynamics of $A_0 = 0.6$, and a triple-photon absorption is observed at $\Omega = 6.5$ (confirmed with the Loschmidt amplitude, not shown). In summary, a clear frequency selection behavior is observed from the energy absorption and site-resolved double occupancy enhancement. The quasiparticle picture for the selective dynamics can be different for different pump frequencies.

To make the laser frequency selection in the dynamical behavior more clear, we plot the site-resolved double occupation as a function of time with different laser intensities in Fig. 5, with the Loschmidt amplitude (see also Sec. V) as a function of ω plotted in the third row. For laser frequency $\Omega = 3.2$, the double occupancy of the A site remains nearly unchanged

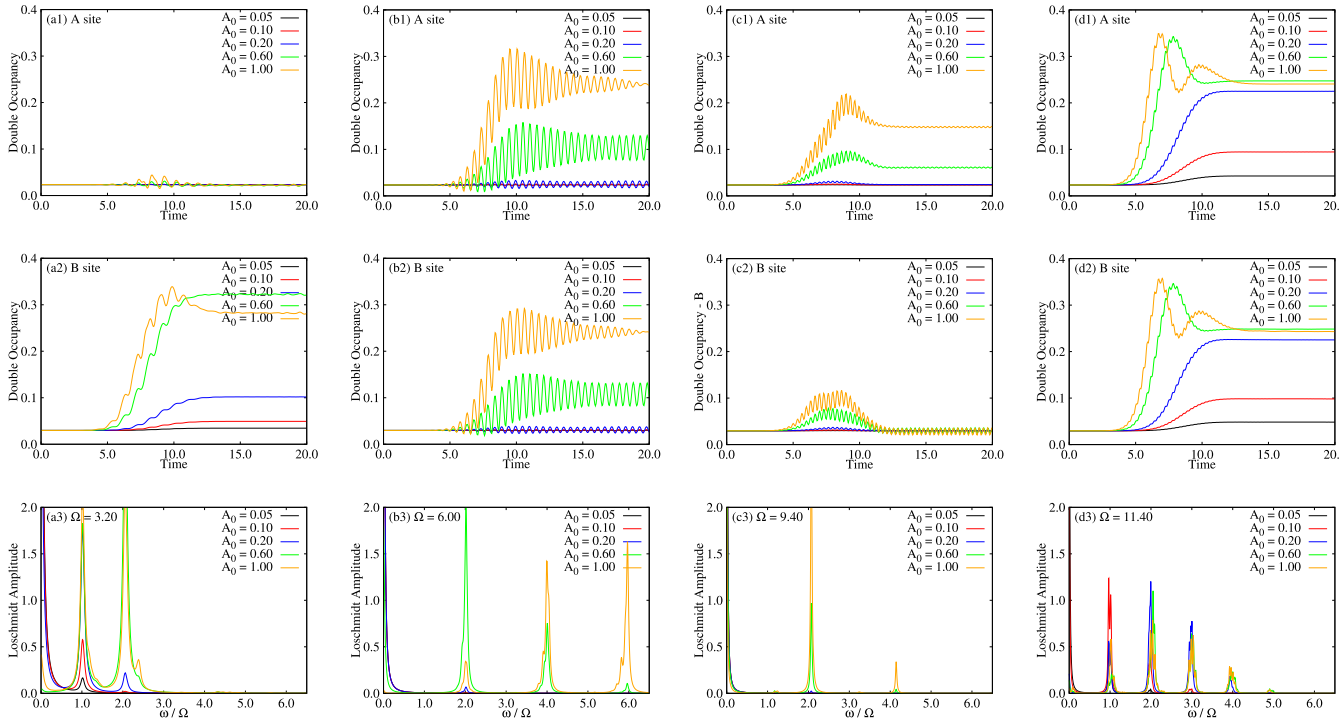

FIG. 5. The time evolution of site-dependent double occupancy and the Loschmidt amplitude for the Hubbard superlattice with fixed site-dependent Coulomb interaction strength $U_b = 3.0$ and $U_a = 18.0$ for different laser amplitudes A_0 and frequency Ω. [(a1)–(a3)] $\Omega = 3.2$, [(b1)–(b3)] $\Omega = 6.0$, [(c1)–(c3)] $\Omega = 9.4$, and [(d1)–(d3)] $\Omega = 11.4$, respectively. The broadening factor is set as $\eta = 0.1$ for the Loschmidt amplitude.

while the B site is significantly enhanced with increased laser intensity. For laser frequency $\Omega = 8.0$ (not shown), the double occupancy of both the A and B sites are unchanged with light. The physics can be explained using the quasiparticle picture of photonic excitation in Ref. [24]. For laser frequency $\Omega = 11.40$, the double occupancy of both A sites and B sites are strongly enhanced. For laser frequency $\Omega = 6.0$, we find that the double occupancy does not change for small laser intensity $A_0 = 0.05, 0.10, 0.20$, while for $A_0 = 0.60, 1.00$, the double occupancy of both A and B sites increase in a similar fashion, which can be explained as multiphoton processes. The multiphoton processes can be identified as double-photon processes by looking at the Loschmidt amplitude, peaking at $2\Omega, 4\Omega, 6\Omega$. Further, the oscillation frequency of double occupancy at long-time regime is independent of the laser intensity, which is different from the Rabi-like behavior (oscillation frequency increase with laser intensity) observed in the pumped two-dimensional Hubbard cluster [21]. At a laser frequency $\Omega = 9.4$, the characterized two-photon process is a one-photon process from the lower Hubbard band of A sites to the upper Hubbard band of B sites, with a subsequent excitation to upper Hubbard band of A sites.

V. THE GENERALIZED LOSCHMIDT AMPLITUDE

In the context of site-selective doublon-holon dynamics, it is important to know which energies will contribute significantly to the double occupancy enhancement of the A sites or the B sites after the laser pulse has passed ($t = 40.0$ used here). To this end, we followed previous work [26] and defined the generalized Loschmidt amplitude with respect to energy and a site-resolved double occupancy,

$$L_{\hat{H}\hat{D}_\alpha}(\omega, D, t) = \sum_{m,n} \langle\psi(t)|E_n\rangle\langle E_n|D_m\rangle\langle D_m|\psi(t)\rangle \times \delta(\omega - E_n)\delta\big(D - D_m^\alpha\big), \tag{9}$$

where $\hat{D}_\alpha = \sum_{i\in\alpha} \hat{n}_{i\uparrow}\hat{n}_{i\downarrow}$ ($\alpha = a, b$ for the A, B sublattices) and $\hat{D}_\alpha|D_m\rangle = D_m^\alpha|D_m\rangle$, with $|D_m\rangle$ the many-body Fock basis with double occupancy $D_m = D_m^a + D_m^b$. Here $|E_n\rangle$ are energy eigenstates of the Hamiltonian with eigenvalue E_n. Due to the fact that the eigenspectrum and eigenstates of double occupancy are *a priori* known, a computational cheaper way to obtain the same information as Eq. (9) is using projectors [26],

$$L_H(\omega, \hat{P}_m) = \sum_n \langle\psi(t)|E_n\rangle\langle E_n|\hat{P}_m|\psi(t)\rangle\delta(\omega - E_n), \tag{10}$$

where $\hat{P}_m = |D_m\rangle\langle D_m|$ is the projector operator onto states with double occupancy, $D_m \in \{0, 1, 2, \ldots, N/2\}$, with N the number of sites in the one-dimensional chain,

$$\sum_{D_m=0}^{N/2} L_H(\omega, \hat{P}_m) = L(\omega). \tag{11}$$

The total double occupancy is expressed as

$$\sum_{D_m=0}^{N/2} D_m \int d\omega L_H(\omega, \hat{P}_m) = \langle\hat{D}\rangle. \tag{12}$$

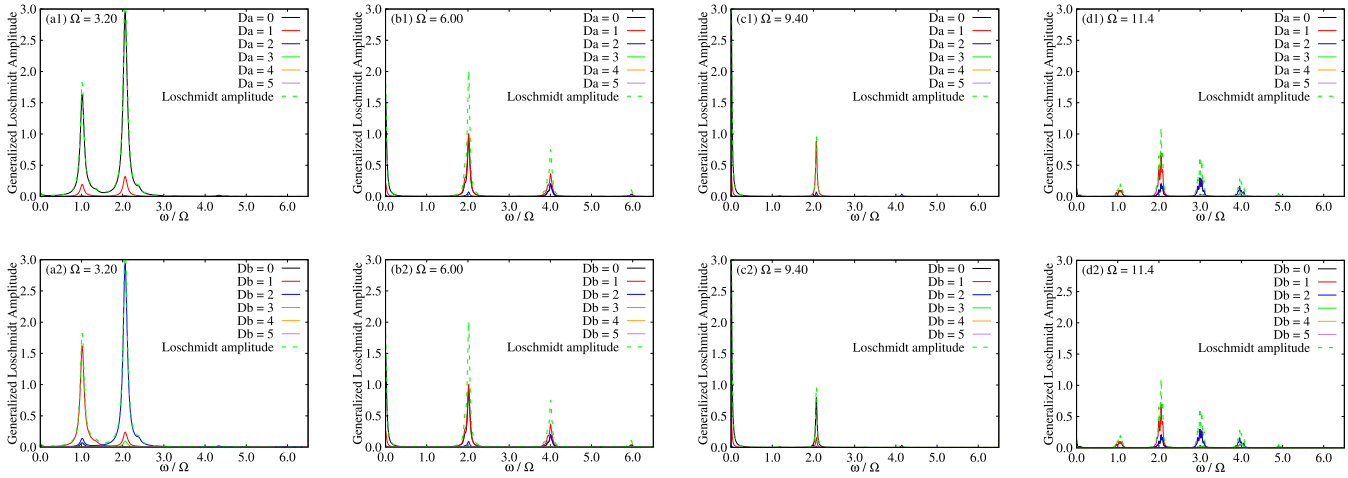

FIG. 6. The double occupancy and generalized Loschmidt amplitude for the Hubbard superlattice with fixed site-dependent Coulomb interaction strength $U_b = 3.0$ and $U_a = 18.0$. These are plotted as a function of energy for different laser frequencies, [(a1) and (a2)] $\Omega = 3.2$, [(b1) and (b2)] $\Omega = 6.0$ [(c1) and (c2)] $\Omega = 9.4$, and [(d1) and (d2)] $\Omega = 11.4$, respectively. The green dashed line is the Loschmidt amplitude, which is a guide to the eye for the sum rule in Eq. (11). The broadening factor is set as $\eta = 0.1$.

The site-resolved double occupancy is

$$\sum_{D_m=0}^{N/2} D_m^{\alpha} \int d\omega L_H(\omega, \hat{P}_m) = \langle \hat{D}_{\alpha} \rangle, \tag{13}$$

where $\alpha = a, b$.

In Fig. 6, we plot the generalized Loschmidt amplitude as a function laser frequency, where the laser amplitude is fixed at $A_0 = 0.60$. For laser frequency $\Omega = 3.2$, the single- and double-photon processes will induce a hopping within the $D_a = 0$ subspace, while the single-photon process will include the state with one double occupancy in the B sublattice, and two-photon processes will induce two double occupancies on the B sites. As a result, the A-site double occupancy does not change and the B-site double occupancy is enhanced.

For laser frequency $\Omega = 6.0$, the single-photon processes are absent and only double-photon process will enhance the $D_a = 1$ subspace. Note that a four-photon process is a sequential two-photon process (one following the other). For laser frequency $\Omega = 9.4$, single-photon processes are absent and only a double-photon process will enhance the $D_b = 0$ subspace and the $D_a = 1$ subspace. Here again the four-photon process is a sequential two-photon process. For laser frequency $\Omega = 11.4$, single-photon processes are observed and a single-photon will enhance the $D_b = 1$ subspace, and the $D_a = 1$ subspace. Here yet again the multiphoton processes are a sequential one-photon process.

VI. CONCLUSION AND DISCUSSION

In this paper, we study the laser driven doubon-holon dynamics in the Hubbard superlattice with spatially modulated (staggered) on site Coulomb interaction. The Coulomb interaction parameters are set as $U_a = 18.0$ and $U_b = 3.0$, for odd and even sites of the one-dimensional chain with periodic boundary conditions adopted. In equilibrium, the site-resolved density of states is studied and shown to exhibit four peaks with lower and upper Hubbard bands and two hybridization peaks. Within linear response theory, we find two main resonance frequencies ($\Omega = 3.2$ and $\Omega = 11.4$) by studying the linear absorption spectrum.

Focusing on the dynamics of the site-resolved double occupancy, we study the time evolution of double occupancy at the A and B sites in the plane of the laser intensity and frequency. For small laser intensity, the system is in the linear response regime, where the resonance frequencies are $\Omega = 3.2$ and $\Omega = 11.4$. At $\Omega = 3.2$, the double occupancy of the A sites remain approximately unchanged, while the double occupancy of the B sites is largely enhanced. The site-resolved doublon-holon dynamics observed above is due to the fact that the upper hybridization band of the A sites is mostly singly occupied, while the upper Hubbard band of the B sites is mostly doubly occupied. At $\Omega = 11.4$, the double occupancy of both A sites and B sites are increased simultaneously by the laser, which is explained as a resonant excitation from the lower Hubbard band of the A(B) sites to upper the Hubbard band of the B(A) sites. For higher laser intensity beyond the linear response regime, multiphoton processes play an important role in the doublon-holon dynamics.

At $\Omega = 6.0$, the double occupancy of the A and B sites remain almost unchanged (oscillating around their equilibrium value at time $t = 0.0^-$) for laser intensity $A_0 = 0.05, 0.10, 0.20$, while for laser intensity $A_0 = 0.6, 1.0$, the double occupancy of both A and B sites increase simultaneously. We conclude that the double-photon processes at $\Omega = 6.0$ for high laser intensity will induce hopping events observed for single-photon processes around $\Omega = 11.4$. Furthermore, at $\Omega = 9.4$, the double occupancy of the A sites is increased significantly while that of the B sites remain almost unchanged, which is what we observed in site-resolved doublon-holon dynamics.

The physical picture for $\Omega = 9.4$ is different from the one for $\Omega = 3.2$, where one hopping event is introduced to explain the dynamics. The phenomena for $\Omega = 9.4$ is explained with two subsequent hopping events: the hopping from the lower Hubbard band of A sites to the upper Hubbard band of B

sites, followed by a second hopping from the upper Hubbard band of B sites to the upper Hubbard band of A sites. The physical pictures described above have been confirmed by direct evaluation of the Loschmidt amplitudes. Taking all these results together, we can conclude that our theoretical study suggests strategies to engineer the doublon-holon dynamics with specified laser parameters.

In summary, the nonequilibrium site-selective doublon-holon dynamics we study is an analog of the orbital-selective Mott transition [50–53] in multiband Hubbard models. In the latter, transport properties in different orbits are selectively influenced by the Coulomb interaction. We are currently undertaking a comparison between site-selective dynamics out-of-equilibrium and orbit-selective transport behavior under equilibrium conditions. Additionally, our investigation reveals site-selective doublon-holon dynamics in the ionic Hubbard model (not illustrated), where one sublattice experiences enhanced doublon occupancy compared to the other, accompanied by an increase in charge-density wave order. The nonequilibrium physics of the ionic Hubbard model will be addressed in a separate study.

ACKNOWLEDGMENTS

We acknowledge helpful discussions with Tao Li, Huan Li, and Xiaojun Zheng. We gratefully acknowledge funding from the Natural Science Foundation of Guangxi Province Grants No. GuiKe AD20297045, No. 2020GXNSFAA297083 and the National Natural Science Foundation of China (Grants No. 11904143, No. 12174168, No. 12247101, and No. 12364022). G.A.F. gratefully acknowledges funding from U.S. National Science Foundation Grant No. DMR-2114825 and the Alexander von Humboldt Foundation.

APPENDIX A: POSITION OF LOWER AND UPPER HUBBARD BAND OF THE HUBBARD SUPERLATTICE

In the homogeneous one-band Hubbard model at half-filling, the positions of the lower and upper Hubbard bands are situated at $-U/2$ and $U/2$ in equilibrium, which can be understood by calculating the lesser Green's function and greater Green's function in the strong Coulomb interaction limit.

The lesser Green's function is defined as

$$G^{<}_{\uparrow}(\omega) = -\sum_{n} \frac{\langle \Psi_g | c^{\dagger}_{\uparrow} | n \rangle \langle n | c_{\uparrow} | \Psi_g \rangle}{\omega + i\eta - (E_0 - E_n)}, \tag{A1}$$

where E_0 and $|\Psi_g\rangle = |\uparrow, \downarrow, \uparrow, \downarrow, \dots\rangle$ are the ground-state energy and vector in the subspace $(N_\uparrow, N_\downarrow)$ and E_n and $|n\rangle$ are the eigenenergy and eigenvector in the subspace $(N_\uparrow - 1, N_\downarrow)$. As a result, the energy difference $E_0 - E_n$ constitutes the position of the lower Hubbard band. The greater Green's function is defined as

$$G^{>}_{\uparrow}(\omega) = +\sum_{m} \frac{\langle \Psi_g | c_{\uparrow} | m \rangle \langle m | c^{\dagger}_{\uparrow} | \Psi_g \rangle}{\omega + i\eta - (E_m - E_0)}, \tag{A2}$$

where E_0 and $|\Psi_g\rangle$ are the ground-state energy and vector in the subspace $(N_\uparrow, N_\downarrow)$ and E_m and $|m\rangle$ are the eigenenergy and eigenvector in the subspace $(N_\uparrow + 1, N_\downarrow)$. As a result, the energy difference $E_m - E_0$ constitutes the position of the upper Hubbard band with one more doubly occupied site.

For the half-filled Hubbard superlattice with staggered Coulomb interactions, its atomic limit Hamiltonian in one unit cell is written as

$$H_{\rm loc} = U_a(n_{a\uparrow} - 1/2)(n_{a\downarrow} - 1/2) + U_b(n_{b\uparrow} - 1/2)(n_{b\downarrow} - 1/2). \tag{A3}$$

The ground-state $|\uparrow_a, \downarrow_b\rangle$ ($|\downarrow_a, \uparrow_b\rangle$) energy in the $(N_\uparrow = 1, N_\downarrow = 1)$ subspace is $-(U_a + U_b)/4$. For the A sublattice (where the newly added or deleted electron is from the A site), in subspace $(N_\uparrow = 0, N_\downarrow = 1)$, the ground-state energy is $(U_a - U_b)/4$, which implies the lower Hubbard band is situated at $-U_a/2$. In subspace $(N_\uparrow = 2, N_\downarrow = 1)$, the ground-state energy is $(U_a - U_b)/4$, where the upper Hubbard band is situated at $U_a/2$. For the B sublattice (where the newly added or deleted electron is from the B site), at subspace

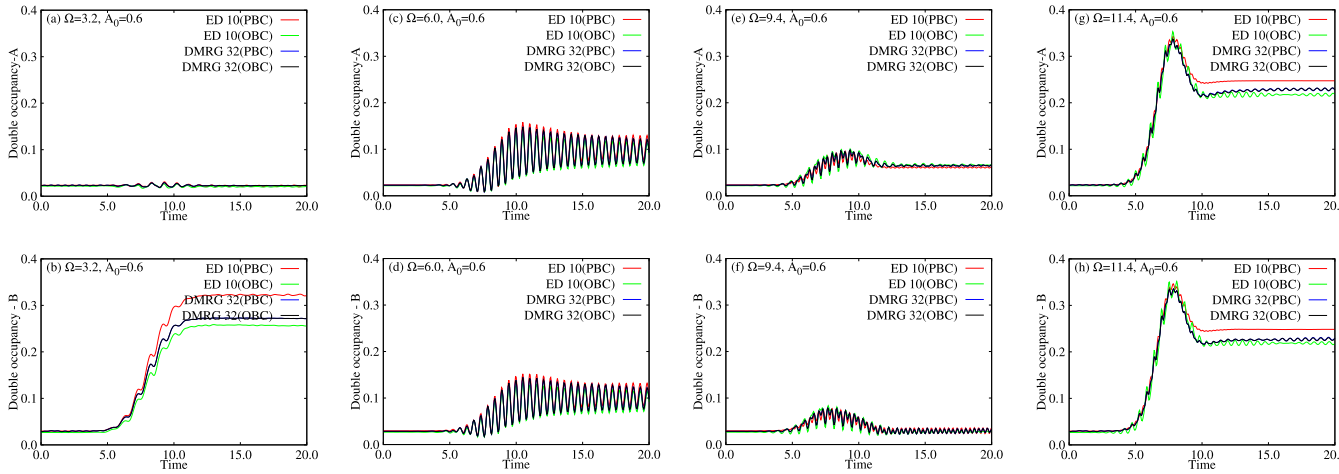

FIG. 7. Density matrix renormalization group (DMRG) calculations compared against exact diagonalizaton for the Hubbard super-lattice with fixed site-dependent Coulomb interaction strength $U_b = 3.0$ and $U_a = 18.0$, the time evolution of site-dependent double occupancy. [(a) and (b)] $\Omega = 3.2$, [(c) and (d)] $\Omega = 6.0$, [(e) and (f)] $\Omega = 9.4$, and [(g) and (h)] $\Omega = 11.4$ for A sites and B sites, respectively. For DMRG, open boundary conditions (OBC) and periodic boundary conditions (PBC) are employed, respectively.

$(N_\uparrow = 1, N_\downarrow = 0)$, the ground-state energy is $(U_b - U_a)/4$, where the lower Hubbard band is situated at $-U_b/2$. In subspace $(N_\uparrow = 1, N_\downarrow = 2)$, the ground-state energy is $(U_b - U_a)/4$, where the upper Hubbard band is situated at $U_b/2$.

APPENDIX B: FINITE-SIZE EFFECTS

To determine the finite-size effects in the nonequilibrium system, we compare our exact diagonalization (10 sites) results of the pumped one-dimensional Hubbard supperlattice chain with the density matrix renormalization group (DMRG) theory (32 sites) using Itensor [54,55]. For both open boundary condition (OBC) and periodic boundary condition (PBC), the DMRG calculations with a 32 site chain is carried out up to five finite-system sweeps keeping up to $m = 500$ states in the equilibrium calculation. The discarded weight is of order 10^{-8}. In the real-time DMRG calculation, we choose the time interval as $\delta t = 0.05$ and only one finite-system sweep is executed. The system parameters are $U_a = 18.0$, $U_b = 3.0$, and $A_0 = 0.6$. The laser frequency is set as $\Omega = 3.2$ (single-photon process) in Figs. 7(a) and 7(b), $\Omega = 6.0$ (double-photon process) in Figs. 7(c) and 7(d), $\Omega = 9.4$ (double-photon process) in Figs. 7(e) and 7(f), and $\Omega = 11.4$ (single-photon process) in Figs. 7(g) and 7(h). The one-dimensional chain with PBC and OBC are employed, respectively. The double occupancy calculated with DMRG (32 sites) and exact diagonalization (10 sites) show good agreement with each other, which indicates that the finite-size effects on the evolution of double occupancy in this work are not severe.

[1] H. Aoki, N. Tsuji, M. Eckstein, M. Kollar, T. Oka, and P. Werner, Nonequilibrium dynamical mean-field theory and its applications, Rev. Mod. Phys. **86**, 779 (2014).

[2] C. Giannetti, M. Capone, D. Fausti, M. Fabrizio, F. Parmigiani, and D. Mihailovic, Ultrafast optical spectroscopy of strongly correlated materials and high-temperature superconductors: A non-equilibrium approach, Adv. Phys. **65**, 58 (2016).

[3] M. Heyl, Dynamical quantum phase transitions: A review, Rep. Prog. Phys. **81**, 054001 (2018).

[4] A. de la Torre, D. M. Kennes, M. Claassen, S. Gerber, J. W. McIver, and M. A. Sentef, *Colloquium:* Nonthermal pathways to ultrafast control in quantum materials, Rev. Mod. Phys. **93**, 041002 (2021).

[5] T. Mori, T. N. Ikeda, E. Kaminishi, and M. Ueda, Thermalization and prethermalization in isolated quantum systems: A theoretical overview, J. Phys. B: At. Mol. Opt. Phys. **51**, 112001 (2018).

[6] J. Berges, A. Rothkopf, and J. Schmidt, Nonthermal fixed points: Effective weak coupling for strongly correlated systems far from equilibrium, Phys. Rev. Lett. **101**, 041603 (2008).

[7] A. Chiocchetta, A. Gambassi, S. Diehl, and J. Marino, Dynamical crossovers in prethermal critical states, Phys. Rev. Lett. **118**, 135701 (2017).

[8] D. Fausti, R. I. Tobey, N. Dean, S. Kaiser, A. Dienst, M. C. Hoffmann, S. Pyon, T. Takayama, H. Takagi, and A. Cavalleri, Light-induced superconductivity in a stripe-ordered cuprate, Science **331**, 189 (2011).

[9] A. Cavalleri, Photo-induced superconductivity, Contemp. Phys. **59**, 31 (2018).

[10] M. Budden, T. Gebert, M. Buzzi, G. Jotzu, E. Wang, T. Matsuyama, G. Meier, Y. Laplace, D. Pontiroli, M. Riccò, F. Schlawin, D. Jaksch, and A. Cavalleri, Evidence for metastable photo-induced superconductivity in K_3C_{60}, Nat. Phys. **17**, 611 (2021).

[11] E. Rowe, B. Yuan, M. Buzzi, G. Jotzu, Y. Zhu, M. Fechner, M. Först, B. Liu, D. Pontiroli, M. Riccò, and A. Cavalleri, Resonant enhancement of photo-induced superconductivity in K_3C_{60}, Nat. Phys. **19**, 1821 (2023).

[12] S. Dal Conte, C. Giannetti, G. Coslovich, F. Cilento, D. Bossini, T. Abebaw, F. Banfi, G. Ferrini, H. Eisaki, M. Greven, A. Damascelli, D. Van Der Marel, and F. Parmigiani, Disentangling the electronic and phononic glue in a high- T_c superconductor, Science **335**, 1600 (2012).

[13] K. A. Al-Hassanieh, F. A. Reboredo, A. E. Feiguin, I. González, and E. Dagotto, Excitons in the one-dimensional Hubbard model: A real-time study, Phys. Rev. Lett. **100**, 166403 (2008).

[14] F. Hofmann and M. Potthoff, Doublon dynamics in the extended Fermi-Hubbard model, Phys. Rev. B **85**, 205127 (2012).

[15] Y. Murakami, S. Takayoshi, T. Kaneko, Z. Sun, D. Golež, A. J. Millis, and P. Werner, Exploring nonequilibrium phases of photo-doped Mott insulators with generalized Gibbs ensembles, Commun. Phys. **5**, 23 (2022).

[16] M. Innerberger, P. Worm, P. Prauhart, and A. Kauch, Electron-light interaction in nonequilibrium: exact diagonalization for time-dependent Hubbard Hamiltonians, Eur. Phys. J. Plus **135**, 922 (2020).

[17] S. Ejima, T. Kaneko, F. Lange, S. Yunoki, and H. Fehske, Photoinduced η -pairing at finite temperatures, Phys. Rev. Res. **2**, 032008(R) (2020).

[18] S. Ejima, F. Lange, and H. Fehske, Nonequilibrium dynamics in pumped Mott insulators, Phys. Rev. Res. **4**, L012012 (2022).

[19] C. Shao, T. Tohyama, H.-G. Luo, and H. Lu, Photoinduced charge carrier dynamics in Hubbard two-leg ladders and chains, Phys. Rev. B **99**, 035121 (2019).

[20] K. Sugimoto and S. Ejima, Pump-probe spectroscopy of the one-dimensional extended Hubbard model at half filling, Phys. Rev. B **108**, 195128 (2023).

[21] J. Okamoto and F. Peronaci, Floquet prethermalization and Rabi oscillations in optically excited Hubbard clusters, Sci. Rep. **11**, 17994 (2021).

[22] L. G. G. V. Dias da Silva, G. Alvarez, and E. Dagotto, Dynamics of doublon-holon pairs in Hubbard two-leg ladders, Phys. Rev. B **86**, 195103 (2012).

[23] A. Kauch, P. Worm, P. Prauhart, M. Innerberger, C. Watzenböck, and K. Held, Enhancement of impact ionization in Hubbard clusters by disorder and next-nearest-neighbor hopping, Phys. Rev. B **102**, 245125 (2020).

[24] F. Maislinger and H. G. Evertz, Impact ionization and multiple photon absorption in the two-dimensional photoexcited Hubbard model, Phys. Rev. B **105**, 045114 (2022).

[25] P. Gazzaneo, T. M. Mazzocchi, J. Lotze, and E. Arrigoni, Impact ionization processes in a photodriven Mott insulator:

Influence of phononic dissipation, Phys. Rev. B **106**, 195140 (2022).
[26] C. Watzenböck, M. Wallerberger, L. Ruzicka, P. Worm, K. Held, and A. Kauch, Photoexcitations in the Hubbard model: Generalized Loschmidt amplitude analysis of impact ionization in small clusters, Phys. Rev. B **106**, 085135 (2022).
[27] M. Fabrizio, A. O. Gogolin, and A. A. Nersesyan, From band insulator to Mott insulator in one dimension, Phys. Rev. Lett. **83**, 2014 (1999).
[28] T. Paiva and R. R. dos Santos, Electronic correlations in one-dimensional superlattices, Phys. Rev. Lett. **76**, 1126 (1996).
[29] T. Paiva and R. R. dos Santos, Metal-insulator transition in one-dimensional Hubbard superlattices, Phys. Rev. B **58**, 9607 (1998).
[30] T. Paiva and R. R. dos Santos, Magnetism in one-dimensional Hubbard superlattices, Phys. Rev. B **62**, 7007 (2000).
[31] T. Paiva and R. R. dos Santos, Charge-density waves in one-dimensional Hubbard superlattices, Phys. Rev. B **65**, 153101 (2002).
[32] C.-B. Duan and W.-Z. Wang, Incommensurate charge correlation and phase diagram of the one-dimensional superlattice Hubbard model at half-filling, J. Phys.: Condens. Matter **22**, 345601 (2010).
[33] L.-L. Zhang, J. Huang, C.-B. Duan, and W.-Z. Wang, Structure-dependent metal– insulator transition in one-dimensional Hubbard superlattice, Chinese Phys. B **24**, 077101 (2015).
[34] V. J. Emery, Strong-coupling field theory and soliton doping in a one-dimensional copper-oxide model, Phys. Rev. Lett. **65**, 1076 (1990).
[35] S. Dag, S. Tongay, T. Yildirim, E. Durgun, R. T. Senger, C. Y. Fong, and S. Ciraci, Half-metallic properties of atomic chains of carbon–transition-metal compounds, Phys. Rev. B **72**, 155444 (2005).
[36] R. Yamazaki, S. Taie, S. Sugawa, and Y. Takahashi, Submicron spatial modulation of an interatomic interaction in a Bose-Einstein condensate, Phys. Rev. Lett. **105**, 050405 (2010).
[37] T. Saitou, A. Koga, and A. Yamamoto, Metal–insulator transition in optical lattice system with site-dependent interactions, J. Supercond. Nov. Magn. **26**, 1771 (2013).
[38] A. Koga, T. Saitou, and A. Yamamoto, Mott transitions in the Hubbard model with spatially modulated interactions, J. Phys. Soc. Jpn. **82**, 024401 (2013).
[39] A.-T. Hoang, T.-H.-Y. Nguyen, T.-T.-T. Tran, and D.-A. Le, Two-component fermions in optical lattice with spatially alternating interactions, J. Phys. Soc. Jpn. **85**, 104702 (2016).
[40] A. Georges, G. Kotliar, W. Krauth, and M. J. Rozenberg, Dynamical mean-field theory of strongly correlated fermion systems and the limit of infinite dimensions, Rev. Mod. Phys. **68**, 13 (1996).
[41] R. Mondaini and T. Paiva, Magnetism, transport, and thermodynamics in two-dimensional half-filled Hubbard superlattices, Phys. Rev. B **95**, 075142 (2017).
[42] H. Lu, S. Sota, H. Matsueda, J. Bonča, and T. Tohyama, Enhanced charge order in a photoexcited one-dimensional strongly correlated system, Phys. Rev. Lett. **109**, 197401 (2012).
[43] J. Okamoto, Time-dependent spectral properties of a photoexcited one-dimensional ionic Hubbard model: an exact diagonalization study, New J. Phys. **21**, 123040 (2019).
[44] T. Kaneko, T. Shirakawa, S. Sorella, and S. Yunoki, Photoinduced η pairing in the Hubbard model, Phys. Rev. Lett. **122**, 077002 (2019).
[45] T. J. Park and J. C. Light, Unitary quantum time evolution by iterative Lanczos reduction, J. Chem. Phys. **85**, 5870 (1986).
[46] N. Mohankumar and S. M. Auerbach, On time-step bounds in unitary quantum evolution using the Lanczos method, Comput. Phys. Commun. **175**, 473 (2006).
[47] M. Balzer, N. Gdaniec, and M. Potthoff, Krylov-space approach to the equilibrium and nonequilibrium single-particle Green's function, J. Phys.: Condens. Matter **24**, 035603 (2012).
[48] C. Moler and C. Van Loan, Nineteen dubious ways to compute the exponential of a matrix, twenty-five years later, SIAM Rev. **45**, 3 (2003).
[49] D. M. Kennes, C. Karrasch, and A. J. Millis, Loschmidt-amplitude wave function spectroscopy and the physics of dynamically driven phase transitions, Phys. Rev. B **101**, 081106(R) (2020).
[50] E. Gull, O. Parcollet, P. Werner, and A. J. Millis, Momentum-sector-selective metal-insulator transition in the eight-site dynamical mean-field approximation to the Hubbard model in two dimensions, Phys. Rev. B **80**, 245102 (2009).
[51] M. Vojta, Orbital-selective Mott transitions: Heavy fermions and beyond, J. Low Temp. Phys. **161**, 203 (2010).
[52] L. de' Medici, G. Giovannetti, and M. Capone, Selective Mott physics as a key to iron superconductors, Phys. Rev. Lett. **112**, 177001 (2014).
[53] D. Tusi, L. Franchi, L. F. Livi, K. Baumann, D. Benedicto Orenes, L. Del Re, R. E. Barfknecht, T.-W. Zhou, M. Inguscio, G. Cappellini, M. Capone, J. Catani, and L. Fallani, Flavour-selective localization in interacting lattice fermions, Nat. Phys. **18**, 1201 (2022).
[54] M. Fishman, S. R. White, and E. M. Stoudenmire, The ITensor-Software Library for tensor network calculations, SciPost Phys. Codebases, 4 (2022).
[55] M. Yang and S. R. White, Time-dependent variational principle with ancillary Krylov subspace, Phys. Rev. B **102**, 094315 (2020).